Aerospace Science and Technology 177 (2026) 112247

Contents lists available at ScienceDirect

Aerospace Science and Technology

journal homepage: www.elsevier.com/locate/aescte

Semi-analytical formation-flying control in J_2-perturbed eccentric orbits

Wei-Ting Chien [a], Afonso Botelho [b], Bruno Ribeiro [b], Kieran Hayward [c], Leonard Felicetti [a,*]

[a] Cranfield University, College Rd, Wharley End, Bedford MK43 0AL, UK
[b] Deimos Engenharia, Indra Space, Av. Columbano Bordalo Pinheiro 75, 9 A1, 1070-061 Lisboa, Portugal
[c] Deimos Space UK, Indra Space, First Floor, AIRSPEED 1, 151 Eighth St, Harwell Oxford, Didcot OX11 0RL, UK

ARTICLE INFO

Communicated by Cummings Russell

Keywords:
Spacecraft formation flying
Semi-analytical solution
GNC
Optimal control

ABSTRACT

This paper presents a methodology for quasi-fuel-optimal control of the relative motion in Earth-orbiting spacecraft formations in J_2-perturbed eccentric orbits using impulsive maneuvers. A closed-form expression describing the inverse relative dynamics with multiple impulsive maneuvers over a defined time window is derived, enabling a semi-analytical approach for obtaining quasi-optimal solutions under a path-minimization assumption. The combined guidance and control formulation, as described by the closed-form expression, is parameterized in terms of quasi non-singular mean relative orbital elements (ROEs) and leverages a linearized J_2-perturbed relative motion model for state prediction using a state transition matrix (STM). The proposed method extends prior ROE-based semi-analytical impulsive-control formulations to the case of J_2-perturbed eccentric orbits. This approach provides geometric insights into secular and long-period effects within the finite reconfiguration windows and is applicable to orbits with arbitrary eccentricity.

1. Introduction

The advancement of Earth-orbiting spacecraft formation flying requires autonomous, fuel-efficient, and flexible reconfiguration of relative motion. Precise relative positioning of multiple spacecraft is essential for advanced distributed sensing and for supporting rendezvous and proximity operations, such as Active Debris Removal (ADR) and On-Orbit Servicing (OOS) activities, including spacecraft maintenance and refuelling. These missions require onboard relative orbit control systems capable of rapidly responding to dynamic conditions, ensuring real-time decision-making with minimal ground intervention. Given the trend toward smaller satellite platforms in future commercial missions, such control systems must also remain computationally efficient. Accordingly, the objective of this work is to develop a computationally efficient quasi-fuel-optimal control formulation for formation reconfiguration that extends prior ROE-based impulsive-control methods to the case where J2 perturbations and orbit eccentricity are considered simultaneously. In this work, quasi-fuel-optimality is interpreted in terms of minimizing total impulsive delta-v.

A leading approach for relative orbit control is the use of slowly time-varying ROEs as relative motion state parametrization, which provide geometric insight into relative orbits and enable the development of control strategies that ensure both safety and efficiency. A variation of ROE, known as Quasi-Non-Singular Relative Orbital Elements, was first introduced by D'Amico [1]. This state representation is capable of handling singularities that arise in near-circular orbits, making it applicable to a wider range of orbital configurations. D'Amico assumed an impulsive control scheme with the concepts of in-plane and out-of-plane reconfiguration, which are crucial for effectively managing satellite relative motion.

Gaias and D'Amico [2] expanded upon these concepts by developing a general formulation for formation reconfiguration using multi-impulsive maneuvers over a finite reconfiguration period, based on linearized dynamics and the inversion of relative motion equations. This formulation is developed using a layered structure involving interdependent optimization problems, including a global guidance layer and the intermediate local control problem [3]. The guidance layer determines the intermediate state configurations to facilitates the transition from the initial to the desired final states within the prescribed time window, while the control layer determines the size and location of impulsive maneuvers required to implement these variations in the state space over a short time interval [4]. Their study provided insight into

* Corresponding author.
E-mail addresses: weitingchien1994@outlook.com (W.-T. Chien), adbotelho@indracompany.com (A. Botelho), baribeiro@indracompany.com (B. Ribeiro), kjfulton@indracompany.com (K. Hayward), leonard.felicetti@cranfield.ac.uk (L. Felicetti).

https://doi.org/10.1016/j.ast.2026.112247
Received 24 August 2025; Received in revised form 12 March 2026; Accepted 28 March 2026
Available online 29 March 2026
1270-9638/© 2026 The Author(s). Published by Elsevier Masson SAS. This is an open access article under the CC BY license (http://creativecommons.org/licenses/by/4.0/).

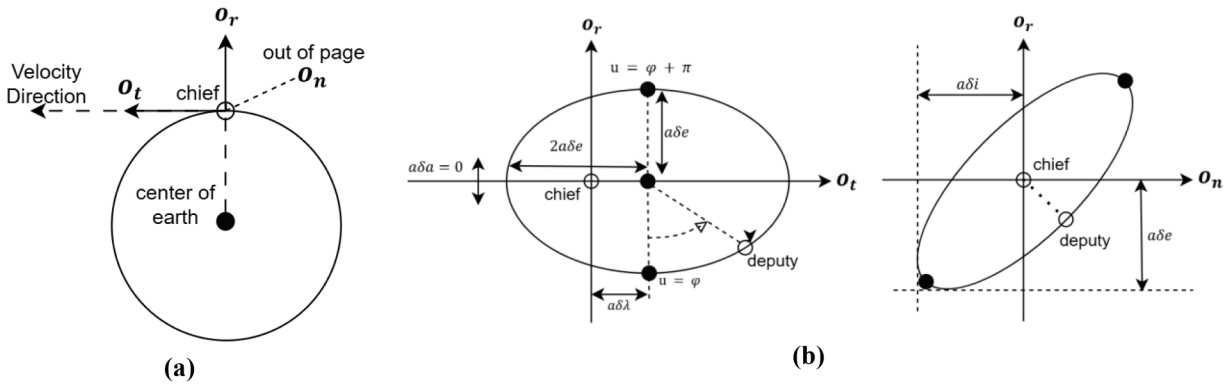


Fig. 1. Hill Frame definition **(a)** and relative orbit geometry described by quasi-nonsingular ROE for circular chief orbit **(b)**. Adapted from [1].

the delta-v cost and the favorable maneuver locations for non-perturbed near-circular orbits.

Chernick and D'Amico [4] further extended this line of research by deriving closed-form optimal solutions for multi-impulsive reconfiguration in unperturbed eccentric orbits and J_2-perturbed near-circular orbits. These optimal solutions are based on path minimization, under the assumption that corrections are primarily dominated by the relative eccentricity vector for in-plane reconfiguration.

Other related developments have expanded the analytical and semi-analytical treatment of relative motion and control in perturbed and eccentric-orbit settings. Delurgio and D'Amico [8] extended the closed-form ROE-based framework to spacecraft swarms in eccentric orbits using reachable-set concepts, while Sasaki [9] developed linear time/parameter-varying ROE models with emphasis on continuous controllability for low-thrust applications. In a broader rendezvous and formation-flying context, Peters [10] considered guidance formulations for elliptical orbits, and Hunter and D'Amico [11] proposed a robust closed-form framework for drag-propulsive control. Additional studies have also addressed relative motion and control in J_2-perturbed eccentric-orbit environments using Cartesian or LVLH-based formulations rather than ROEs. For example, Willis and D'Amico [12] addressed analytical relative-motion modelling in Cartesian form for J_2-perturbed eccentric orbits, Kuiack and Ulrich [13] developed nonlinear analytical equations and associated guidance formulations in the same setting, and earlier studies such as Cao and Chen [14] and Sabatini et al. [15] considered control design in J_2-perturbed environments under different assumptions and control frameworks. In addition, Sengupta et al. [16] developed an averaged (secular) relative-motion description for formation flight near perturbed orbits, which further illustrates the role of secular perturbations in long-term relative dynamics.

Building on these prior works [2–4], the present paper extends the family of semi-analytical impulsive ROE control solutions reported in [4] to the case of simultaneously J_2-perturbed and eccentric orbits, which, to the best of the authors' knowledge, has not been addressed exactly in the literature. In particular, the proposed approach develops a semi-analytical formulation for spacecraft-formation control within the ROE framework that accounts for both secular J_2 effects and the additional complexity associated with an eccentric chief orbit. The present method follows the general maneuver structure adopted in earlier ROE-based studies, namely three tangential maneuvers for in-plane correction and one normal maneuver for out-of-plane correction [2,4], while extending the analytical treatment to the J_2-perturbed eccentric-orbit case considered here.

The ROE framework has been demonstrated to be effective for formulating control strategies that are fuel-efficient and computationally viable, making it well suited to onboard implementation in future space missions. Within this context, the present study examines the combined effects of J_2 perturbation and orbit eccentricity in the impulsive-planning stage, where previous formulations within this solution family addressed these effects separately. Numerical simulations and comparative analysis demonstrate that the proposed control schemes improve reconfiguration accuracy relative to previously established methods [4]. Furthermore, this study evaluates the cross-coupling between in-plane and out-of-plane elements arising from the use of the J_2-perturbed STM and the control input matrix for eccentric orbits. The results indicate that the dominant source of cross-coupling is the control input matrix and that its effect can be mitigated by sequential out-of-plane and in-plane maneuver planning.

2. Theoretical background

This section contains two review topics: the Gauss variational equations and the quasi-non-singular ROE. The quasi-non-singular ROE are used for error description of absolute and relative motion propagation as well as parameter in the formation-keeping control algorithm. The Gauss variational equations are used in the derivation of relative orbit propagation based on averaging theory and on the control input matrix that maps external acceleration to the change of ROE. The quasi-non-singular ROE are used as the parameters describing the relative motion states.

2.1. Gauss Variational Equations

The Gauss Variational Equations (GVE) describe the evolution of the classical orbital elements, $\boldsymbol{\alpha} = [a,e,i,\Omega,\omega,\nu]$, of a satellite orbiting Earth under the influence of perturbative forces translated to Radial-Tangential-Normal (RTN) frame. The GVE are applicable to both conservative (J_2) and non-conservative perturbation such as maneuver, drag and Solar Radiation Pressure (SRP). It is used to derive the J_2 perturbed dynamic model of relative motion and the control input matrix for the change of ROE. As defined by Vallado [5]:

$$
\begin{aligned}
\frac{da}{dt} &= \frac{2}{n\sqrt{1-e^2}}\left\{e\sin(\nu)d_R + \frac{p}{r}d_T\right\}\\
\frac{de}{dt} &= \frac{\sqrt{1-e^2}}{na}\left\{\sin(\nu)d_R + \left(\cos(\nu) + \frac{e+\cos(\nu)}{1+e\cos(\nu)}\right)d_T\right\}\\
\frac{di}{dt} &= \frac{r\cos(\theta)}{na^2\sqrt{1-e^2}}d_N\\
\frac{d\Omega}{dt} &= \frac{r\sin(\theta)}{na^2\sqrt{1-e^2}\sin(i)}d_N\\
\frac{d\omega}{dt} &= \frac{\sqrt{1-e^2}}{nae}\left\{-\cos(\nu)d_R + \sin(\nu)\left(1+\frac{r}{p}\right)d_T\right\} - \frac{r\cot(i)\sin(\theta)}{h}d_N\\
\frac{d\nu}{dt} &= \frac{h}{r^2} + \frac{1}{eh}\{p\cos(\nu)\}d_R - (p+r)\sin(\nu)d_T
\end{aligned}
\tag{1}
$$

where disturbance accelerations **d** (from manoeuvring, drag, SRP, J_2)

consist of components in the radial (d_R), transverse (d_T), and normal (d_N) directions and n, h, r, p are the mean motion, specific angular momentum, orbital radius and semi-latus rectum respectively. In addition, r denotes the instantaneous orbital radius and $a,\ e, i,\ \Omega,\ \omega,\ \nu$ denotes the Keplerian elements of semi-major axis, eccentricity, inclination, Right Ascension of the Ascending Node, argument of perigee and true anomaly respectively. The system of equation can be converted in matrix form where $\mathbf{G}_{[6,3]}$ is the GVE matrix, $\mathbf{c}$ is a term independent of the disturbances, and both are functions of the absolute orbit elements $\boldsymbol{\alpha}$

$$\dot{\boldsymbol{\alpha}} = \mathbf{G}(\boldsymbol{\alpha})\mathbf{d} + \mathbf{c}(\boldsymbol{\alpha}) \tag{2}$$

2.2. Quasi-nonsingular ROE

Relative motion is commonly described and visualized using the Hill Frame (also known as Local-Vertical-Local-Horizontal Frame or RTN Frame), which provides an intuitive and direct perspective on relative motion in relations to the absolute dynamics of the chief orbit. This motion can be directly represented as relative position and velocity in rectilinear coordinates within the Hill Frame, or it can be represented by parametrization such as Relative Orbital Elements (ROE). The Hill Frame simplifies the control of relative motion due to its correlation with the dynamics of the chief's orbit. As shown in Fig. 1, the Hill Frame is centered at the chief's center of mass, with the radial vector pointing outward from Earth, the normal vector perpendicular to the orbital plane, and the tangential vector aligned with the orbital velocity if the orbit is circular.

The ROE are constructed by combining absolute orbital elements to describe the relative motion of spacecraft in formation flying. Unlike the rapidly changing RTN coordinates, ROE vary slowly over time relative to the orbital period, with the exception of anomalies. In this work, a variation of the ROE, termed the Quasi-Non-Singular Relative Orbit Elements, is used, following the definitions provided by D'Amico [1]:

$$\delta\boldsymbol{\alpha} = \begin{pmatrix} \delta a \\ \delta\lambda \\ \delta e_x \\ \delta e_y \\ \delta i_x \\ \delta i_y \end{pmatrix} = \begin{pmatrix} \delta a \\ \delta\lambda \\ \delta e\cos\varphi \\ \delta e\sin\varphi \\ \delta i\cos\vartheta \\ \delta i\sin\vartheta \end{pmatrix} = \begin{pmatrix} \dfrac{a_d - a_c}{a_c} \\ u_d - u_c + (\Omega_d - \Omega_c)\cos(i_c) \\ e_d\cos(\omega_d) - e_c\cos(\omega_c) \\ e_d\sin(\omega_d) - e_c\sin(\omega_c) \\ i_d - i_c \\ (\Omega_d - \Omega_c)\sin(i_c) \end{pmatrix} \tag{3}$$

which consist of the in-plane ROE relative semi-major axis δa, relative mean longitude $\delta\lambda$, relative eccentricity vector $\delta\mathbf{e} = \left(\delta e_x, \delta e_y\right)^T$ and out-of-plane ROE—relative inclination vector $\delta\mathbf{i} = \left(\delta i_x, \delta i_y\right)^T$. The subscript c and d refer to chief and deputy respectively. Take note that the mean argument of latitude $u = \omega + M, e_x = e\cos\omega$ and $e_y = e\sin\omega$, where M is the mean anomaly. This ROE definition avoids singularity that arise from circular orbits and enables effective handling of both circular and eccentric orbits. Additionally, as shown in Fig. 1, the ROE provides meaningful geometric insights into the relative orbit, such as its size and orientation.

2.3. Linearized dynamic model

This section introduces various linearized propagation models of ROE, expressed in STM. In general, ROE can be propagated as follows:

$$\delta\boldsymbol{\alpha}_f = \boldsymbol{\Phi}_{f,0}\delta\boldsymbol{\alpha}_0 \tag{4}$$

where $\boldsymbol{\Phi}_{f,0}$ is the state transition matrix from initial to final point, $\delta\boldsymbol{\alpha}_0$ is the initial ROE state and $\delta\boldsymbol{\alpha}_f$ is the final ROE state. The simplest form of linearized relative dynamic, which assume Keplerian dynamic with no perturbation, results in the following STM [1]

$$\boldsymbol{\Phi}_{f,0} = \begin{pmatrix} 1 & 0 & 0 & 0 & 0 & 0 \\ -\dfrac{3}{2}n\Delta\tau & 1 & 0 & 0 & 0 & 0 \\ 0 & 0 & 1 & 0 & 0 & 0 \\ 0 & 0 & 0 & 1 & 0 & 0 \\ 0 & 0 & 0 & 0 & 1 & 0 \\ 0 & 0 & 0 & 0 & 0 & 1 \end{pmatrix} \tag{5}$$

where only $\delta\lambda$ varies due to different semi-major axes ($\delta a \neq 0$) between chief and deputy. Here the subscript 'c' and 'd' are dropped and the related orbital parameter such as n refer to chief orbit element. In the absence of perturbations, the absolute Keplerian elements of both the chief and deputy remain constant, with the exception of the anomalies. Consequently, all states in the ROE defined in (3) remain invariant over time, except for the mean argument of latitude, u, for which an approximated rate is obtained by linearization about small δa[1].

The ROE based equations of relative motion under disturbance acceleration (perturbation, maneuver) can be derived through the GVE in (2), expressed in matrix form and applied to each individual satellite as [4]:

$$\dot{\delta\boldsymbol{\alpha}} = \frac{\partial\delta\boldsymbol{\alpha}}{\partial\boldsymbol{\alpha}_c}\dot{\boldsymbol{\alpha}}_c + \frac{\partial\delta\boldsymbol{\alpha}}{\partial\boldsymbol{\alpha}_d}\dot{\boldsymbol{\alpha}}_d = \frac{\partial\delta\boldsymbol{\alpha}}{\partial\boldsymbol{\alpha}_c}(\mathbf{G}(\boldsymbol{\alpha}_c)(\mathbf{d}_{J_2}(\boldsymbol{\alpha}_c) + \mathbf{R}_{cd}\mathbf{d}_{\mathrm{m}}) + \mathbf{c}(\boldsymbol{\alpha}_c)) + \frac{\partial\delta\boldsymbol{\alpha}}{\partial\boldsymbol{\alpha}_d}(\mathbf{G}(\boldsymbol{\alpha}_d)\mathbf{d}_{J_2}(\boldsymbol{\alpha}_d) + \mathbf{c}(\boldsymbol{\alpha}_d)) \tag{6}$$

where $\mathbf{d}_{J_2}$ is the acceleration due to J_2 and $\mathbf{d}_{\mathrm{m}}$ is the acceleration due to the thrusters (in the chief LVLH), $\mathbf{R}_{cd}$ is the rotation matrix from the chief's to the deputy's RTN frame, which can be assumed as identity matrix due to proximity of the absolute orbit elements between chief and

deputy in most close formation flying scenario.

By applying J_2 perturbation function to d and performing a first-order Taylor expansion on the resultant equations of relative motion in (6) for $\mathbf{d}_{\mathrm{m}} = 0$, the J_2 perturbed ROE STM is given by [6]:

$$\boldsymbol{\Phi}_{f,0} = \begin{pmatrix} 1 & 0 & 0 & 0 & 0 & 0 \\ -\frac{7}{2}\kappa EP\tau - \frac{3}{2}n\tau & 1 & \kappa e_{x0}FGP\tau & \kappa e_{y0}FGP\tau & -\kappa FS\tau & 0 \\ \frac{7}{2}\kappa e_{yf}Q\tau & 0 & \cos(\dot{\omega}\tau) - 4\kappa e_{x0}e_{yf}GQ\tau & -\sin(\dot{\omega}\tau) - 4\kappa e_{y0}e_{yf}GQ\tau & 5\kappa e_{yf}S\tau & 0 \\ -\frac{7}{2}\kappa e_{xf}Q\tau & 0 & \sin(\dot{\omega}\tau) + 4\kappa e_{x0}e_{xf}GQ\tau & \cos(\dot{\omega}\tau) + 4\kappa e_{y0}e_{xf}GQ\tau & -5\kappa e_{xf}S\tau & 0 \\ 0 & 0 & 0 & 0 & 1 & 0 \\ \frac{7}{2}\kappa S\tau & 0 & 0 & -4\kappa e_{x0}GS\tau & 2\kappa T\tau & 1 \end{pmatrix} \tag{7}$$

$$= \frac{3}{4}J_2R_{e\sqrt{\mu}}^2, \quad \eta = \sqrt{1-|e|^2}, \quad \kappa = \frac{\gamma}{7a^2\eta^4}, \quad G = \frac{1}{\eta^2}, \quad \dot{\omega} = \kappa Q, \quad \tau = t_f - t_0$$

$$E = 1+\eta, \quad F = 4+3\eta, \quad T = \sin^2(i), \quad e_{x,0} = e\cos(\omega), \quad e_{x,f} = e\cos(\omega + \dot{\omega}\tau)$$

$$P = 3\cos^2(i) - 1, \quad Q = 5\cos^2(i) - 1, \quad S = \sin(2i), \quad e_{y,0} = e\sin(\omega), \quad e_{y,f} = e\sin(\omega + \dot{\omega}\tau)$$

part of the first-order linearization and does not imply physical co-location or collision between the chief and deputy spacecraft. Here, $\boldsymbol{\Gamma}_m$ is a function of the chief orbital elements, the subscript m denotes the m-th impulsive maneuver, and the subscripts c and d refer to the chief and deputy, respectively. For the general case of arbitrary chief eccentricity, $\boldsymbol{\Gamma}_m$ is defined as follows:

$$\boldsymbol{\Gamma}_m = \frac{1}{na}\begin{pmatrix} \frac{2}{\eta}e\sin\nu_m & \frac{2}{\eta}(1+e\cos\nu_m) & 0 \\ -\eta\left[\frac{2\eta}{1+e\cos\nu_m} - \frac{(\eta-1)\cos\nu_m}{e}\right] & \frac{\eta(1-\eta)\sin\nu_m}{e}\left(1+\frac{1}{1+e\cos\nu_m}\right) & 0 \\ \eta\sin\theta_m & \eta\frac{(2+e\cos\nu_m)\cos\theta_m + e_{x,m}}{1+e\cos\nu_m} & \frac{\eta e_{y,m}\sin\theta_m}{\tan(i)(1+e\cos\nu_m)} \\ -\eta\cos\theta_m & \eta\frac{(2+e\cos\nu_m)\sin\theta_m + e_{y,m}}{1+e\cos\nu_m} & -\frac{\eta e_{x,m}\sin\theta_m}{\tan(i)(1+e\cos\nu_m)} \\ 0 & 0 & \frac{\cos\theta_m}{1+e\cos\nu_m} \\ 0 & 0 & \frac{\sin\theta_m}{1+e\cos\nu_m} \end{pmatrix} \tag{9}$$

2.4. Control input matrix

The change of ROE due to an instantaneous impulsive maneuver with a change of velocity $\delta\mathbf{v}_m$ applied to the deputy spacecraft along the RTN direction at time t_m can be described by the control input matrix $\boldsymbol{\Gamma}_m$, which is derived by taking $\mathbf{d}_m = \delta\mathbf{v}_m\delta(t_m)$, where $\delta(t_m)$ is the Dirac delta function, $\mathbf{d}_{J_2} = 0$, and $\mathbf{c} = 0$ and solving (6) [7]:

$$\Delta\delta\boldsymbol{\alpha}_m = \left[\frac{\partial\delta\boldsymbol{\alpha}}{\partial\boldsymbol{\alpha}_d}\mathbf{G}(\boldsymbol{\alpha}_d)\right]\Big|_{\boldsymbol{\alpha}_d=\boldsymbol{\alpha}_c}\delta\mathbf{v}_m = \boldsymbol{\Gamma}_m(\boldsymbol{\alpha}_c)\begin{pmatrix}\delta v_{\mathrm{R},m}\\ \delta v_{\mathrm{T},m}\\ \delta v_{\mathrm{N},m}\end{pmatrix} \tag{8}$$

It should be noted that the condition $\boldsymbol{\alpha}_d = \boldsymbol{\alpha}_c$ is introduced solely as where $\theta_m = \omega_m + \nu_m$ is the true argument of latitude of chief at the point of maneuver. Take note of the potential singularity arise when $e = 0$, the term $\frac{\eta(1-\eta)}{e}$ approaches 0 as $e \to 0$, although it is numerically stable down to e = 1e-6. The control input matrix $\boldsymbol{\Gamma}_m$ can be simplified if we assumed circular chief orbit and is given by

$$\boldsymbol{\Gamma}_m = \frac{1}{na}\begin{pmatrix} 0 & 2 & 0 \\ -2 & 0 & 0 \\ \sin(u_m) & 2\cos(u_m) & 0 \\ -\cos(u_m) & 2\sin(u_m) & 0 \\ 0 & 0 & \cos(u_m) \\ 0 & 0 & \sin(u_m) \end{pmatrix} \tag{10}$$

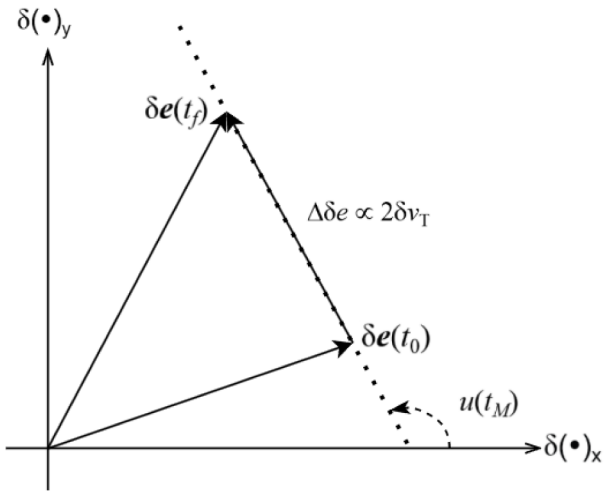


Fig. 2. Notional illustration of effects of impulsive along-track maneuvers in ROE space. Adapted from [4].

It can be observed from (10) that the control problem can be simplified by decoupling the in-plane and out-of-plane maneuvers for near-circular orbits. While cross-coupling terms exist in the case of eccentric orbits, as shown in (9), the simplified approach based on plane separation can still be applied through sequential compensation. This work assumes that the out-of-plane maneuver is performed independently from the in-plane maneuvers. The effect of the out-of-plane maneuver on the in-plane ROE is subtracted from the desired change in the in-plane ROE if performed before the in-plane maneuvers, and vice versa.

3. Controller framework

A reconfiguration from a given initial relative orbit to a desired final one can be defined as the transition $\boldsymbol{\alpha}_0 \rightarrow \boldsymbol{\alpha}_f$ over the finite-time interval to span $u_0 \rightarrow u_f$. The explicit involvement of the final time does not reduce the generality of the treatment but allows addressing more practical scenarios in which a reconfiguration has to cope with possible requirements coming from the space segment [5].

The overall guidance and control problem over the reconfiguration period is formulated by incorporating the effects of multiple impulses under the linearizing assumptions. In the following, subscripts 1 to p denote the impulse sequence, with maneuver i applied at time t_i. Given the initial ROE state $\delta\boldsymbol{\alpha}(t_0)$, the final state after p impulsive delta-v is given by

$$\delta\boldsymbol{\alpha}_f = \boldsymbol{\Phi}_{f,0}\delta\boldsymbol{\alpha}(t_0) + \boldsymbol{\Phi}_{f,1}\boldsymbol{\Gamma}_1\Delta\delta\mathbf{v}_1 + \cdots + \boldsymbol{\Phi}_{f,p}\boldsymbol{\Gamma}_p\Delta\delta\mathbf{v}_p \tag{11}$$

Given the initial chief orbital elements $\boldsymbol{\alpha}_{c,0}$ (to construct $\boldsymbol{\Phi}$ and $\boldsymbol{\Gamma}$) and the initial ROE $\delta\boldsymbol{\alpha}_0$, the reconfiguration problem is defined by a desired final ROE, $\delta\boldsymbol{\alpha}_f$, and the final reconfiguration time t_f. With these reconfiguration parameters, the control and guidance problem to be solved is [7]

$$\Delta\delta\overline{\alpha} = \delta\boldsymbol{\alpha}_f - \boldsymbol{\Phi}_{f,0}\delta\boldsymbol{\alpha}_0 = \boldsymbol{\Phi}_{f,1}\boldsymbol{\Gamma}_1\Delta\delta\mathbf{v}_1 + \cdots + \boldsymbol{\Phi}_{f,p}\boldsymbol{\Gamma}_p\Delta\delta\mathbf{v}_p \tag{12}$$

Where $\Delta\delta\overline{\alpha}$ is the pseudo-states that represent the desire change of ROE by impulsive maneuvers after accounting for the evolution of initial ROE over the reconfiguration period.

3.1. Optimal control problem

Closed-form solutions for fuel-optimal relative orbit control maneuvers are sought. Specifically, an optimal semi-analytical solution is derived for reconfigurations characterized by $|\Delta\delta\mathbf{e}| > |\Delta\delta a|$. This work directly extends previous studies conducted in unperturbed eccentric orbits [3]. Previous study [4] has shown, the most efficient maneuver direction for achieving a desired change in the ROE can be determined by comparing the normalized effects of a unit-sized Δv on the ROE. For instance, the maximum change in $\Delta\delta a$ achieved with an unit input tangential maneuver is $\frac{2}{\eta}(1+e)$ at $\nu = 0$, which is more efficient than the $\frac{2}{\eta}e$ achieved with a radial maneuver at $\nu = \frac{\pi}{2}$.

Similarly, the maximum change in $\Delta\delta\mathbf{e}$ achieved with an unit input tangential maneuver is 2η at $\nu = k\pi$, which is twice as efficient compare to the η achieved with a radial maneuver. While the aimed $\Delta\delta\lambda$ can be achieved through a tangential burn by introducing the drift coefficient for the appropriate duration of the reconfiguration. Resulting in the following delta v lower bound characterized by normalized effect of tangential maneuver for $\Delta\delta a$ and $\Delta\delta\mathbf{e}$:

$$\frac{\delta v_{LB}}{na\eta} \approx \max\left(\frac{|\Delta\delta a|}{2(1+e)}, \frac{|\Delta\delta\lambda|}{K(e,\Delta M)}, \frac{|\Delta\delta e|}{2\eta^2}\right) \tag{13}$$

Considering in-plane reconfigurations where $\Delta\delta\mathbf{e}$ correction is dominant, tangential maneuvers are exclusively employed due to their inherent efficiency. Previous work [2] has shown that while two tangential maneuvers may suffice for reconfiguration, they cannot achieve the minimum Δv cost. However, using three tangential maneuvers enables the derivation of analytical or semi-analytical solutions that can achieve the Δv lower bound. This leads to the development of an optimal multi-impulse control scheme consisting of three tangential maneuvers for in-plane reconfiguration and one normal maneuver for out-of-plane reconfiguration.

Finally, the quasi-optimal maneuver locations are found at multiples of half the orbital period ($k\pi$, where k is an integer) from the initial optimal maneuver location. While there is flexibility in the choice of k, a general guideline for multi-impulse maneuver schemes is to schedule the first maneuver as early as possible and the last as late as possible within the reconfiguration period. Additionally, selecting a combination of even and odd values for k is recommended, which allows at least one maneuver on each side of the orbit.

In this work, we adopt the assumption from previous work [4] that minimizing fuel consumption is equivalent to minimizing the path in ROE space from the initial to the final conditions, as illustrated in Fig. 2. While we have not proven that this equivalence holds exactly in the J_2-perturbed eccentric-orbit case, we expect deviations to be small for the reconfiguration windows and regimes considered, and we therefore use this assumption to obtain quasi-optimal maneuver timing and allocation. The cost of any reconfiguration is driven by the largest variation among the relative semi-major axis, relative mean longitude, and relative eccentricity vector. For instance, in the unperturbed case where the correction of $\Delta\delta\mathbf{e}$ dominates in-plane reconfiguration, the optimal maneuver points are located to maintain a constant gradient in the evolution of the relative eccentricity vector $\Delta\delta\mathbf{e}$ throughout the reconfiguration period. This ensures that $\Delta\delta e_x$ and $\Delta\delta e_y$ evolve with constant ratios across all maneuvers, resulting in fuel-efficient solution with minimum path length.

3.2. Near-optimal multi-impulse control

This section focuses on the general formulation of a closed-form expression for near-optimal multi-impulse control, which comprises three tangential maneuvers for in-plane reconfiguration and a single normal maneuver for out-of-plane reconfiguration [2]. Assuming maneuver occurs in a single direction for the reconfiguration of each plane, we begin by analyzing the case of in-plane reconfiguration:

$$\begin{aligned} \boldsymbol{X}_{f,m} &= \boldsymbol{\Phi}_{f,m}\boldsymbol{\Gamma}_m \\ \Delta\delta\mathbf{v}_m &= \begin{pmatrix} \delta v_{R,m} \\ \delta v_{T,m} \\ \delta v_{N,m} \end{pmatrix} = \begin{pmatrix} 0 \\ \delta v_{T,m} \\ 0 \end{pmatrix} \end{aligned} \tag{14}$$

where considering the effect of multiple maneuvers by applying (14) to (12) and accounting only the in-plane ROE:

$$\Delta\delta\overline{\alpha} = \boldsymbol{X}_{f,1}(1:4,2)\delta v_{T,1} + \cdots + \boldsymbol{X}_{f,p}(1:4,2)\delta v_{T,p} = \begin{pmatrix}\boldsymbol{X}_{f,1}(1:4,2) & \cdots & \boldsymbol{X}_{f,p}(1:4,2)\end{pmatrix}\begin{pmatrix}\delta v_{T,1}\\ \vdots \\ \delta v_{T,p}\end{pmatrix}$$
$$\Delta\delta\overline{\alpha}_{[4,1]} = \mathbf{M}_{[4,p]}\delta\overline{\boldsymbol{\nu}}_{[p,1]} \tag{15}$$

Where $\mathbf{M}$ is made up of horizontal stack of 2nd column of $\boldsymbol{\Phi}_{f,m}\boldsymbol{\Gamma}_m$ for $m = 1, 2, \ldots, p$. It should be noted that for out-of-plane reconfiguration the $\mathbf{M}$ and $\delta\overline{\mathbf{v}}$ matrix is constructed with $\boldsymbol{X}_{f,m}(5:6, 3)$ and $\delta v_{N,m}$ respectively. The computation can be simplified by moving all the shared constant term (such as $\frac{1}{na}$) in $\mathbf{M}$ to $\Delta\delta\boldsymbol{\alpha}$, leading to the revised expression:

$$\overline{\mathbf{M}}\delta\overline{\mathbf{v}} = c\Delta\delta\overline{\alpha} \tag{16}$$

Where c is the inverse of the shared constant term in $\mathbf{M}$. The control problem is thus driven by the input $\delta\overline{\alpha}$ and is approached by first determining the points of maneuver based on the path length minimization of the dominant ROE element, which determines $\overline{\mathbf{M}}$, then subsequently solve for $\delta\overline{\mathbf{v}}$. In this work, we assume dominant correction for $\delta\mathbf{e}$ for in-plane reconfiguration.

4. Control in perturbed eccentric orbits

In this section, we will incorporate the effects of secular J_2 perturbation into the relative motion dynamics for an eccentric chief orbit. Given the complexity introduced by these perturbations, a closed-form solution is not feasible, therefore, a semi-analytical approach is presented. The derivation is based on (7) for $\boldsymbol{\Phi}$, which is a function of time and (9) for Control Input Matrix $\boldsymbol{\Gamma}$, which is a function of true anomaly, applying them to the right-hand side of (12). Under J_2 perturbation, the absolute orbit element of chief is no longer invariant and presents additional complexity as the terms in $\overline{\mathbf{M}}$ involves both true anomaly and time, which varies non-linearly. Conversion between the two requires determining the argument of perigee at the point of maneuver which drifts over time due to J_2 perturbation and is a function of time. Hence, an iterative process is required, with the following relations:

$$\tau_{m,0} = t_m - t_0 = \frac{u_m - u_0}{\dot{u}} = \frac{M_m - M_0}{\dot{M}} = \frac{\omega_m - \omega_0}{\dot{\omega}}\quad \dot{M} = n + \kappa\eta P,\quad \dot{\omega} = \kappa Q,\quad \dot{u} = n + \kappa(\eta P + Q),\quad \omega_m = \omega_0 + \dot{\omega}\tau_{m,0}\quad E_m = \frac{e + \cos(\theta_m - \omega_0 - \dot{\omega}\tau)}{1 + e\cos(\theta_m - \omega_0 - \dot{\omega}\tau)},$$
$$M_m = \dot{M}\tau + M_0 = E_m - \sin(E_m)$$

where the J_2 related drift term can be found in [7]. Given the initial chief orbit element $\boldsymbol{\alpha}_{c,0}$, specifically $M_0, \omega_0$and e, we can iteratively find the corresponding $\tau_{m,0}$ of an input θ_m by minimizing the error function:

$$X_{err} = (n + \kappa\eta P)\tau_{m,0} + M_0 - \frac{e + \cos(\theta_m - \omega_0 - \dot{\omega}\tau)}{1 + e\cos(\theta_m - \omega_0 - \dot{\omega}\tau)} + \sin\frac{e + \cos(\theta_m - \omega_0 - \dot{\omega}\tau)}{1 + e\cos(\theta_m - \omega_0 - \dot{\omega}\tau)} \tag{18}$$

With the initial guess approximated to the nearest semi-circle of the orbit plane using mean motion and delta true anomaly:

$$\tau_{m,0} = \frac{\theta_m - \theta_0}{\dot{u}} \tag{19}$$

4.1. Out-of-plane reconfiguration

The term associated with e_x and e_y cancel each other when multiplying the STM with the control input matrix, hence simplifying the system of equations into:

$$\frac{\eta}{na}\frac{\cos(\theta_m)}{1 + e\cos(\nu_m)}\delta v_{N,m} = \Delta\delta\bar{i}_x$$
$$\frac{\eta}{na}\frac{2\kappa T\tau_{f,m}\cos(\theta_m) + \sin(\theta_m)}{1 + e\cos(\nu_m)}\delta v_{N,m} = \Delta\delta\bar{i}_y \tag{20}$$

With the corresponding $\overline{\mathbf{M}}$ and $c\Delta\delta\overline{\alpha}$:

$$\overline{\mathbf{M}} = \begin{pmatrix}\frac{\cos(\theta_m)}{1 + e\cos(\nu_m)} & \frac{2\kappa T\tau_{f,m}\cos(\theta_m) + \sin(\theta_m)}{1 + e\cos(\nu_m)}\end{pmatrix},\quad c\Delta\delta\overline{\alpha} = \frac{na}{\eta}\begin{pmatrix}\delta\bar{i}_x\\ \delta\bar{i}_y\end{pmatrix} \tag{21}$$

We can iteratively solve for the point of maneuver:

$$(\cos(\theta_m))\left(\delta\overline{y} - 2\kappa T\tau_{f,m}\delta\overline{x}\right) = (\sin(\theta_m))\delta\overline{x}$$
$$\tau_{f,m} = t_f - t_m = \tau_{f,0} - \tau_{m,0} \tag{22}$$

With initial guess:

$$\overline{\theta}_m = \arctan\left(\frac{\delta\overline{y}}{\delta\overline{x}}\right)$$
$$\theta_m = \overline{\theta}_m - \left(\frac{\overline{\theta}_m - \theta_0}{\pi}\right)\pi + k \tag{23}$$

For implementation, we need to account for relative correction to ensure that the point of maneuver is after the initial point. Hence $\overline{\theta}_m$ is shifted by multiple of π until its larger than θ_0, resulting in θ_m. For a given guess of θ_m, we can derive the corresponding $\tau_{m,0}$ with (18), which allows us to derive the $\tau_{f,m}$ in (22) given the fixed configuration window t_f that is known. The two values should not be confused: the former refers to the time elapsed from the initial point to the maneuver point and is associated with the control input matrix, while the latter refers to the time elapsed from the maneuver point to the final time within the reconfiguration window and is associated with the STM. The δv_m can subsequently be found by substituting the solution from (22) into the first row of (20) if $\delta\overline{y} = 0$ and the second row if $\delta\overline{x} = 0$.

4.2. In-Plane reconfiguration

For in-plane reconfiguration, the following representation of (7) for STM $\mathbf{\Phi}$, and (9) for Control Input Matrix, $\mathbf{\Gamma}$, is used to improve readability:

$$\mathbf{\Phi}_{f,m} = \begin{pmatrix} 1 & 0 & 0 & 0 & 0 & 0 \\ A_m & 1 & D_m & L_m & -\kappa FS\tau & 0 \\ B_m & 0 & H_m & N_m & 5\kappa e_y fS\tau & 0 \\ C_m & 0 & I_m & R_m & -5\kappa e_x fS\tau & 0 \\ 0 & 0 & 0 & 0 & 1 & 0 \\ \frac{7}{2}\kappa S\tau & 0 & -4\kappa e_x GS\tau & -4\kappa e_y GS\tau & 2\kappa T\tau & 1 \end{pmatrix}$$

$$\mathbf{\Gamma}_m = \frac{1}{na}\begin{pmatrix} \frac{2}{\eta}e\sin\nu_m & X_m & 0 \\ -\eta\left(\frac{2n}{1+e\cos\nu_m} - \frac{(\eta-1)\cos\nu_m}{e}\right) & W_m & 0 \\ \eta\sin\theta_m & Y_m & \frac{\eta e_y \sin\theta_m}{\tan(i)(1+e\cos\nu_m)} \\ -\eta\cos\theta_m & Z_m & -\frac{\eta e_x \sin\theta_m}{\tan(i)(1+e\cos\nu_m)} \\ 0 & 0 & \frac{\eta\cos\theta_m}{1+e\cos\nu_m} \\ 0 & 0 & \frac{\eta\sin\theta_m}{1+e\cos\nu_m} \end{pmatrix} \tag{24}$$

Resulting in the system of equations:

$$\begin{aligned} \sum_{m=1}^{3} X_m \delta\mathbf{v}_m &= na\Delta\delta\overline{\alpha} \\ \sum_{m=1}^{3} (A_m X_m + D_m Y_m + L_m Z_m + W_m)\delta\mathbf{v}_m &= na\Delta\delta\overline{\lambda} \\ \sum_{m=1}^{3} (B_m X_m + H_m Y_m + N_m Z_m)\delta\mathbf{v}_m &= na\Delta\delta\overline{e}_x \\ \sum_{m=1}^{3} (C_m X_m + I_m Y_m + R_m Z_m)\delta\mathbf{v}_m &= na\Delta\delta\overline{e}_y \end{aligned} \tag{25}$$

With the corresponding $\overline{\mathbf{M}}$ and $c\Delta\delta\overline{\alpha}$:

$$\overline{\mathbf{M}} = \begin{pmatrix} X_1 & X_2 & X_3 \\ A_1X_1 + D_1Y_1 + L_1Z_1 + W_1 & A_2X_2 + D_2Y_2 + L_2Z_2 + W_2 & A_3X_3 + D_3Y_3 + L_3Z_3 + W_3 \\ B_1X_1 + H_1Y_1 + N_1Z_1 & B_2X_2 + H_2Y_2 + N_2Z_2 & B_3X_3 + H_3Y_3 + N_3Z_3 \\ C_1X_1 + I_1Y_1 + R_1Z_1 & C_2X_2 + I_2Y_2 + R_2Z_2 & C_3X_3 + I_3Y_3 + R_3Z_3 \end{pmatrix} \tag{26}$$

$$c\Delta\delta\overline{\alpha} = na\begin{pmatrix} \Delta\delta\overline{a} \\ \Delta\delta\overline{\lambda} \\ \Delta\delta\overline{e}_x \\ \Delta\delta\overline{e}_y \end{pmatrix}$$

As per the out-of-plane case, it is important to note that $B_m, C_m, H_m, I_m, N_m, R_m$ are associated with the STM as expressed in (7) and involve $\tau_{f,m}$, ω_m $(e_{x,0}, e_{y,0})$ and ω_f $(e_{x,f}, e_{y,f})$, the latter can be computed at the start given the known initial condition and the final reconfiguration time, while X_i, Y_i, Z_i are associated with the Control Input Matrix expressed in (9) and involve $\tau_{m,0}$ and ω_m. Computing these two sets of terms should be done separately in implementation to avoid confusion. Assuming dominant relative eccentricity vector correction, we can iteratively solve for the points of maneuver with path minimization by

$$(C_mX_m + I_mY_m + R_mZ_m)\Delta\delta\overline{e}_x = (B_mX_m + H_mY_m + N_mZ_m)\Delta\delta\overline{e}_y, \tag{27}$$

with initial guess

$$\begin{aligned} \overline{\theta}_m &= \operatorname{atan}\left(\frac{\Delta\delta\overline{e}_y}{\Delta\delta\overline{e}_x}\right), \\ \theta_m &= \overline{\theta}_m - \left\lfloor\frac{\overline{\theta}_m - \theta_0}{\pi}\right\rfloor\pi + k_m. \end{aligned} \tag{28}$$

$\delta\mathbf{v}$ can subsequently be found by substituting the solution of (27) into (25), followed by the inversion of the $\overline{\mathbf{M}}$ matrix. For implementation, it is ideal to iterate (27) using time or the mean anomaly as the independent variable. This approach is advantageous because converting from the time domain to the true anomaly domain is straightforward, and it also simplifies the derivation of terms associated with both the STM and the control input matrix. The initial guess may be derived from the (28) based on the true anomaly, with the reverse conversion from true anomaly to time only performed once during initialization for each point of the maneuver. Lastly, we know that for a dominant $\delta\mathbf{e}$ correction, the optimal path is achieved via minimal path length of the $\delta\mathbf{e}$ correction, i.e., a straight line. This means the ratio of correction of δe_x and δe_y is the same for all three maneuvers. While this consideration holds true for unperturbed relative dynamics, it may still be used as an approximation for near optimal solution with perturbed relative dynamics, assuming the differences in drift rate due to correctional maneuvers over the configuration time span is significantly lower than the pre-accounted eccentricity drift due to the initial ROE states over the reconfiguration time span. To aid the comprehension on computing the in-plane reconfiguration, a pseudo-code is presented in Algorithm 1, where θ_{error} is the residual of (27), computed as the difference between its left-hand side and right-hand side.

Algorithm

5. Numerical validation

The multi-impulse control scheme derived previously is assessed in numerical simulation through a piecewise propagation procedure. At each prescribed impulse epoch, the simulation is terminated, the terminal state is extracted, and the computed delta-v is applied instantaneously to the deputy spacecraft velocity vector. The subsequent

Algorithm 1
Triple tangential impulse in-plane reconfiguration control algorithm.

Input: $t_f, \delta\alpha_0, \delta\alpha_f, k$
Result: $\Delta\delta\overline{v}, t_m$
Calculate $\Delta\delta\overline{\alpha}, \dot{\omega}, e_{xf}, e_{yf}$ with (12);
for $m = 1$ to 3 do
  while $\theta_{error} > \theta_{tol}$ do
    iterate θ_m, adjust relative to θ_{error}. Initialized with (28) instead for the first iteration;
    Calculate time of maneuver $\tau_{m,0}$ with (18);
    Calculate e_{xm}, e_{ym} and the propagation duration $\tau_{f,m}$ with (12);
    Calculate $C_m, B_m, I_m, H_m, M_m, R_m$ terms with (24);
    Calculate X_m, Y_m, Z_m terms with (24);
    Calculate θ_{error} according to (27);
  end
end
Calculate $\overline{M}$ with (26);
Calculate $\Delta\delta\overline{v}, t_m$ with (16);

Table 1
Proposed Maneuver plan for the out-of-plane test case.

k	Time (s)	θ (rad)	δv_T (m/s)
0	5736	3.242	−0.1404

trajectory is then propagated in a new simulation instance initialised with the updated state and with the start time set equal to the terminal time of the preceding propagation segment. The chief and deputy trajectories are propagated in Simulink using the Aerospace Blockset Orbit Propagator block, employing a variable-step ode45 solver and accounting for the J2 perturbation. The results will then be compared with existing control schemes from the literature [4] using the same implementation, which provide formulations for the cases of unperturbed eccentric and J_2-perturbed circular orbits. Both in-plane and out-of-plane reconfiguration scenarios will be evaluated, with particular emphasis on operations within an orbit with significant J_2 perturbation to examine the effects of this perturbation.

Additionally, the method is evaluated in the general reconfiguration case presented in Section 5.3, which involves both in-plane and out-of-plane maneuvers executed sequentially within a single reconfiguration window. These evaluations will assess the cross-coupling terms between planes, which arise from the STM and the control input matrix, and explore mitigation methods to improve accuracy by compensating the in-plane final target elements based on the results of the out-of-plane maneuver.

5.1. Out-of-plane reconfiguration

This test aims to evaluate the proposed out-of-plane control formulation for J_2 perturbed eccentric orbit described in Section 4.1. An orbit with a large eccentricity is chosen, and to assess its effectiveness under J_2 perturbation, an orbit with pronounced J_2-induced effects on the relative inclination vector is selected.

$$\dot{\delta i_y} = (\dot{\Omega}_d - \dot{\Omega}_c)\sin(i_c), \quad \dot{\Omega} = -\frac{3}{2} J_2 \frac{nR^2}{a^2(1-e^2)^2}\cos(i) \tag{29}$$

As shown in (29), $\dot{\delta i_y}$ is largest at high inclinations as the term $\sin(i_c)$ reaches its maximum and the J_2-induced relative drift term $\dot{\Omega}_d - \dot{\Omega}_c$, caused by the small inclination mismatch between the chief and deputy, is maximized due to the steep gradient of the $\cos(i)$ term. Hence, the initial state and parameters are given as follows:

$$\begin{gathered} \boldsymbol{\alpha}_c = [a_c, e_c, i_c, \omega_c, \Omega_c, \nu_c]^T = [11000km, 0.4, 88^\circ, 5^\circ, 5^\circ, 5^\circ]^T \\ a_c\delta\boldsymbol{\alpha}_0 = [0, 0, 0\text{m}, 0\text{m}, 10\text{m}, 70\text{m}]^T \\ a_c\delta\boldsymbol{\alpha}_f = [0, 0, 0\text{m}, 0\text{m}, 400\text{m}, 120\text{m}]^T \\ k = 0, \quad u_f = 14 \end{gathered} \tag{30}$$

Note that the out-of-plane ROE parameters are selected such that both the magnitude and phase of the relative inclination vector undergo significant change during the reconfiguration. The test case is designed to be as representative as practicable of a meaningful mission profile, here adopted as a departure scenario, while ensuring sufficient variation in the ROE parameters for assessment of the proposed control scheme. The maneuver plan derived by the control solution is summarized in Table 1. Fig. 3 illustrates the deputy's trajectory in the chief's Hill frame, as well as the evolution of the out-of-plane ROE during the reconfiguration interval to achieve the desired ROE. The maneuver results in a significant change in the relative orbit geometry and the effects of J_2-perturbation are clearly observable, as evidenced by the drift of the relative orbit after the maneuver, which is also reflected in the δi_y plot.

As shown in Table 2, the newly derived control scheme produces accurate solutions with sub-meter error when comparing to the Target ROE, resulting in a significant improvement over the previously derived unperturbed eccentric solution [4], which did not account for J_2 effects. A substantial reduction in δi_y error is observed. A comparison is also made with the J_2-perturbed circular model [4], which exhibits significant errors, including errors in δi_x on the order of hundreds of meters. These errors arise primarily from neglecting eccentricity effects, which have a far greater impact than neglecting J_2 perturbations.

5.2. In-plane reconfiguration

This test aims to evaluate the proposed in-plane control formulation for J_2 perturbed eccentric orbit described in Section 4.2. As per previous section, an orbit with a large eccentricity is chosen and a significant $\Delta\delta\lambda$ is introduced to simulate a rendezvous scenario. To assess its effectiveness under J_2 perturbation, an orbit with pronounced J_2-induced effects on the relative eccentricity vector is selected.

$$\dot{\omega} = -\frac{3}{4}\frac{J_2 R_e^2 \sqrt{\mu}}{a^{7/2}\eta^4}\left(5\cos^2 i - 1\right) \tag{31}$$

As per the definition of the eccentricity vector in (3), it is primarily influenced by the drift of the argument of perigee, which, according to (31), is maximized in an equatorial orbit [4]. Hence, a low-inclination orbit is selected, and the initial parameters are chosen as follows:

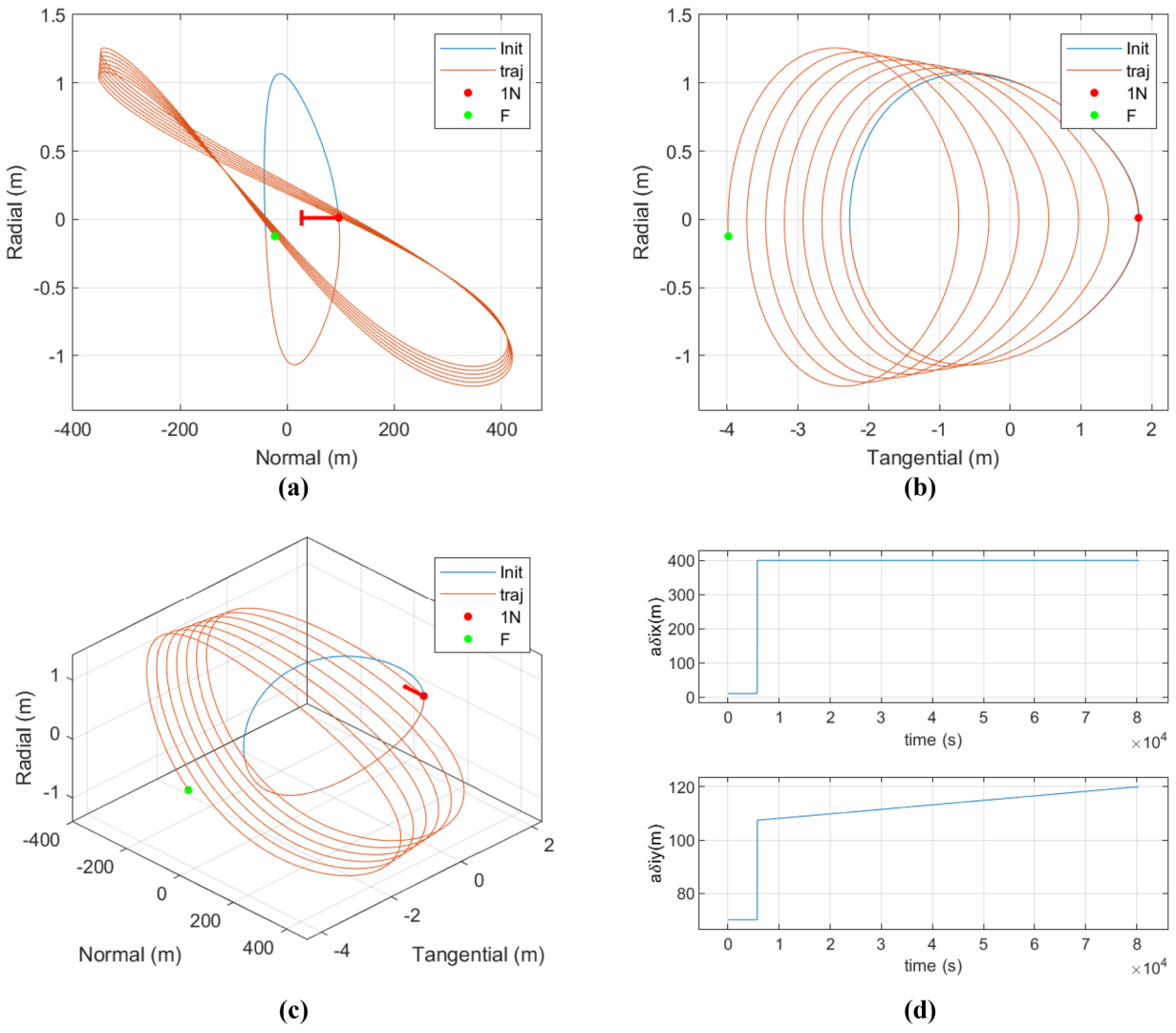


Fig. 3. Deputy relative trajectory in the chief Hill frame during the out-of-plane reconfiguration, with the impulsive maneuver locations and directions indicated in the legend. **(a)** Normal–radial plane. **(b)** Tangential–radial plane. **(c)** Three-dimensional view (radial–tangential–normal). **(d)** Time histories of the normalized out-of-plane ROE components.

Table 2
Comparison of maneuver schemes for out-of-plane test case.

Control Scheme	Achieved (m)		Error (m)	
	$a_c\delta i_x$	$a_c\delta i_y$	$a_c\delta i_x$	$a_c\delta i_y$
Target ROE	400	120	-	-
J_2-perturbed Circular	606.25	143.25	206.25	23.25
Unperturbed Eccentric	400.25	132.00	2.51e-1	12.00
***Proposed* J_2-perturbed Eccentric**	400.16	120.02	1.60e-1	1.57e-2

$$\begin{aligned} \boldsymbol{\alpha}_c &= [a_c, e_c, i_c, \omega_c, \Omega_c, \nu_c]^T = [11000km, 0.4, 10^\circ, 5^\circ, 5^\circ, 5^\circ]^T \\ a_c\delta\boldsymbol{\alpha}_0 &= [0, 10000\text{m}, 0\text{m}, -200\text{m}, 200\text{m}, 0\text{m}]^T \\ a_c\delta\boldsymbol{\alpha}_f &= [5\text{m}, 500\text{m}, 100\text{m}, 0\text{m}, 200\text{m}, 0\text{m}]^T \\ k &= 0, 5, 12 \quad u_f = 15 \end{aligned} \tag{32}$$

Note that the in-plane ROE parameters are selected such that both the magnitude and phase of the relative eccentricity vector undergo significant change during the reconfiguration, while the remaining in-plane ROE components also experience meaningful variation. The test case is selected to be as representative as practicable of a meaningful mission profile, here taken as a far-to-close reconfiguration scenario, while ensuring sufficient variation in the ROE parameters for assessment of the proposed control scheme. The maneuver plan derived by the control solution is summarized in Table 3. Fig. 4 illustrates the deputy's trajectory in the chief's Hill frame, as well as the evolution of the in-plane ROE during the reconfiguration interval to achieve the desired ROE. The 3 tangential impulse and their respective direction are plotted and as indicated in the legend.

Table 3
Proposed Maneuver plan for the in-plane test case.

k	Time (s)	θ (rad)	δv_T (m/s)
0	970	1.325	0.0511
5	31,340	16.605	−0.0397
12	69,766	39.037	−0.0245
Total delta-v			0.115

As shown in Table 4, the newly derived control formulation produces accurate solutions with sub-meter error, except for $\delta\lambda$. The error is likely due to the breakdown of the linearization assumption of small δa during the reconfiguration. The resultant small error in δa accumulates over the reconfiguration period, leading to a cumulative error in $\delta\lambda$. Nevertheless, the new control scheme significantly reduces the overall error compared to the unperturbed eccentric [4] and J2-perturbed circular [4] formulations.

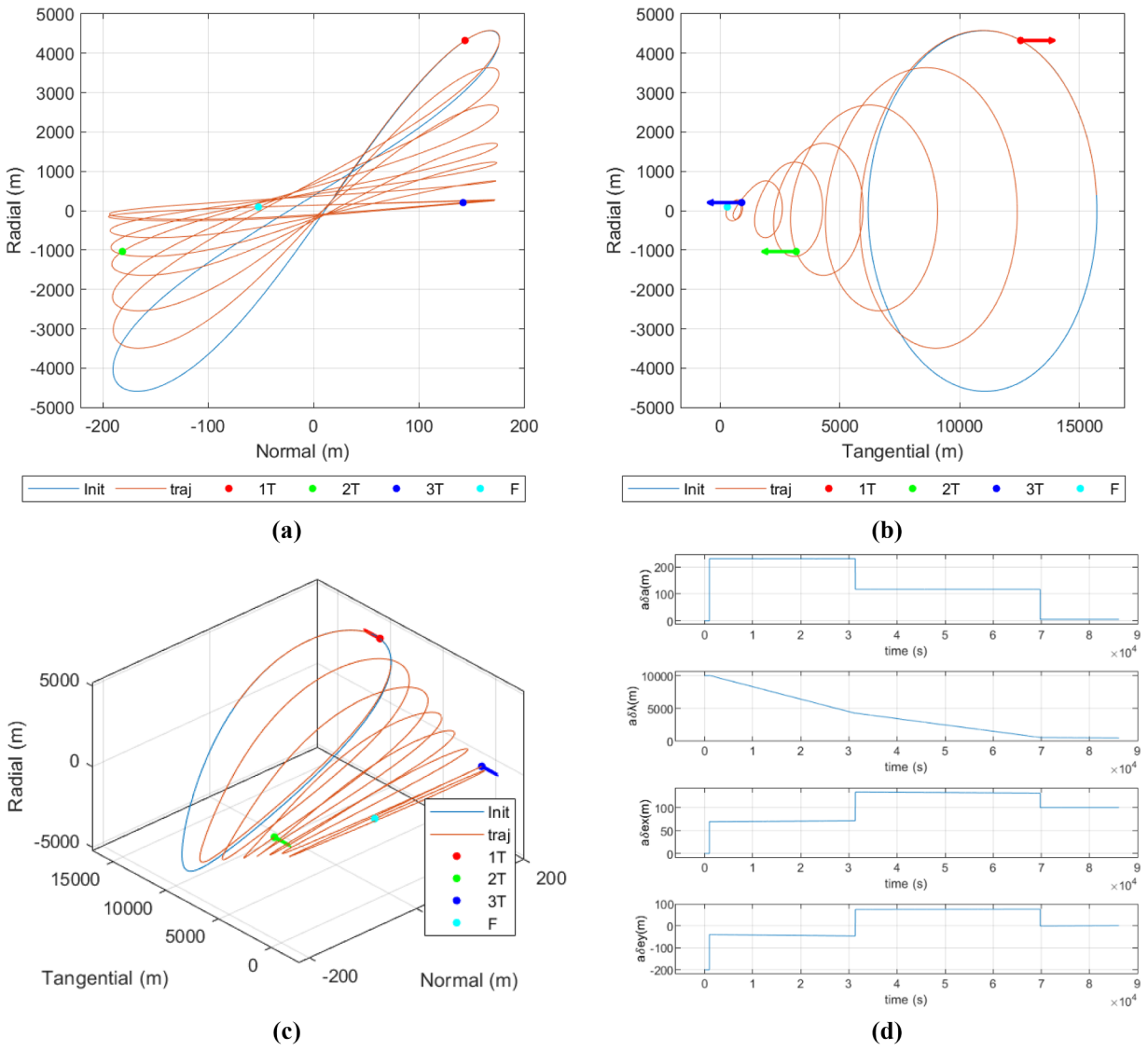


Fig. 4. Deputy relative trajectory in the chief Hill frame during the in-plane reconfiguration, with the impulsive maneuver locations and directions indicated in the legend. **(a)** Normal–radial plane. **(b)** Tangential–radial plane. **(c)** Three-dimensional view (radial–tangential–normal). **(d)** Time histories of the normalized in-plane ROE components.

Table 4
Comparison of maneuver schemes for in-plane test case.

Control Scheme	$a_c\delta a$	Achieved $a_c\delta\lambda$	(m) $a_c\delta e_x$	$a_c\delta e_y$	$a_c\delta a$	Error $a_c\delta\lambda$	(m) $a_c\delta e_x$	$a_c\delta e_y$
Target ROE	5	500	100	0	-	-	-	-
J_2-perturbed Circular	30.95	−162.79	55.65	−37.10	25.94	−662.79	−44.36	−37.10
Unperturbed Eccentric	6.35	−35.34	3.05	−3.19	1.35	−35.34	3.05	−3.19
***Proposed* J_2-perturbed Eccentric**	5.17	494.56	99.93	4.12e-1	1.73e-1	−5.44	−7.25e-2	4.12e-1

5.3. General reconfiguration

The cross-coupling between in-plane and out-of-plane arises in two main ways. First, it is due to the control input matrix $\mathbf{\Gamma}_m$ in (9), specifically the terms $\mathbf{\Gamma}_m(3, 3)$ and $\mathbf{\Gamma}_m(3, 4)$, which result in the out-of-plane maneuver in the normal direction having a direct effect on the in-plane relative eccentricity vector. Second, it is caused by the state transition matrix (STM) in (7), specifically the terms $\mathbf{\Phi}(6, 1)$ and $\mathbf{\Phi}(6, 4)$, where changes of *in*-plane elements affect the out-of-plane elements, and vice versa for $\mathbf{\Phi}(2, 5)$, $\mathbf{\Phi}(3, 5)$, and $\mathbf{\Phi}(4, 5)$. This section evaluates these cross-coupling effects and assess the accuracy of a general reconfiguration involving both in-plane and out-of-plane reconfigurations. The first two tests involve performing individual maneuvers (in- plane and out-of-plane) to examine their effects on the elements of the other plane. The last two tests consist of sequential maneuver planning, where the out-of-plane maneuver is performed first. One test assumes the two maneuvers are independent, while the other includes compensation for the in-plane final ROE based on the results of the out-of-plane maneuver planning. A test case of rendezvous in an eccentric orbit is selected, given the initial and final parameters as:

Table 5
Final achieved ROE for general reconfiguration.

Control Scheme	$a_c\delta a$	$a_c\delta\lambda$	Achieved $a_c\delta e_x$	(m) $a_c\delta e_y$	$a_c\delta i_x$	$a_c\delta i_y$
Initial ROE	0	10,000	200	200	400	400
Target ROE	5	2000	100	100	200	200
OP Only	4.29e-2	10,006	113.75	664.73	200.92	199.52
IP Only	4.98	199.40	100.06	99.65	400.04	400.06
OP and IP without comp	4.99	2001	29.47	543.62	200.66	202.10
OP and IP with comp	5.02	200.10	100.18	99.23	200.68	202.57

Table 6
Normalized ROE error for general reconfiguration.

Control Scheme	$a_c\delta a$	$a_c\delta\lambda$	Error $a_c\delta e_x$	(m) $a_c\delta e_y$	$a_c\delta i_x$	$a_c\delta i_y$
OP Only	−4.96	8006.10	13.75	564.73	9.20e-1	−4.79e-1
IP Only	−1.68e-2	−6.19e-1	5.53e-2	−3.53e-1	200.04	200.06
OP and IP without comp	−1.38e-2	9.50e-1	−70.53	443.62	6.63e-1	2.10
OP and IP with comp	1.98e-2	8.22e-2	1.85e-1	−7.71e-1	6.84e-1	2.57

$$\begin{aligned} \boldsymbol{\alpha}_c &= [a_c, e_c, i_c, \omega_c, \Omega_c, \nu_c]^T = [11000km, 0.4, 10^\circ, 5^\circ, 5^\circ, 5^\circ]^T \\ a_c\delta\boldsymbol{\alpha}_0 &= [0, 10000\text{m}, 200\text{m}, 200\text{m}, 400\text{m}, 400\text{m}]^T \\ a_c\delta\boldsymbol{\alpha}_f &= [5\text{m}, 2000\text{m}, 100\text{m}, 100\text{m}, 200\text{m}, 200\text{m}]^T \\ k_{ip} = 12 \quad k_{op} &= 0,\ 5,\ 12 \quad u_f = 15 \end{aligned} \tag{33}$$

Table 5 presents the achieved ROE for the four test cases, while Table 6 provides the corresponding errors. The terms OP and IP represent out-of-plane and in-plane, respectively. From the "OP Only" results, it can be observed that there is a significant change in the in-plane element of relative eccentricity vector from the initial ROE state. Specifically, a change of 465 m is observed in $a_c\delta e_x$, indicating that the cross-coupling due to the control input matrix is significant and dominant. In contrast, the "OP Only" reconfiguration has minimal effect on the in-plane components of the relative inclination vector, which are primarily influenced by the cross-coupling in the STM terms. This observation is further supported by the third test case, where out-of-plane and in-plane maneuver planning are performed independently but executed together, resulting in a significant error in $a_c\delta\mathbf{e}$. Furthermore, the effect of the cross-coupling terms in the STM becomes significant in $a_c\delta i_y$, with the error increasing from sub-meter levels to 2∼m. This occurs because the out-of-plane maneuver planning does not account for changes in the in-plane ROE due to the in-plane maneuver during the derivation of $\Delta\delta\overline{\alpha}$ in (12).

The fourth test case (OP and IP with compensation) involves first performing out-of-plane maneuver planning and calculating the change in the in-plane elements resulting exclusively from the out-of-plane impulse. This calculation does not account for the evolution of the in-plane elements based on the initial ROE, as described in (12), since they are already accounted of in the out-of-plane maneuver planning using the same initial ROE parameters. Finally, this change in the in-plane ROE is subtracted from the target final ROE for in-plane maneuver planning prior to the planning itself, as outlined in (34). For this test case, the change of in-plane elements is as follows:

$$\begin{aligned} \delta\boldsymbol{\alpha}_{f,ip} &= \delta\boldsymbol{\alpha}_f - \Delta\boldsymbol{\alpha}_{op} \\ \Delta\boldsymbol{\alpha}_{op} &= \boldsymbol{\Phi}_{f,n}\boldsymbol{\Gamma}_n\delta\nu_n \\ a\Delta\boldsymbol{\alpha}_{op} &= [\,0 \quad 1.63 \quad -70.37 \quad 443.71\,]^T \end{aligned} \tag{34}$$

As shown in Table 6, the compensation significantly improves the accuracy of the solution, reducing the error in $a_c\delta e_x$ and $a_c\delta e_y$ to sub-meter levels. However, the error in $a_c\delta i_x$persists. This error could be addressed using a similar compensation strategy as proposed in (34) for out-of-plane to in-plane maneuvers. Such an approach, however, would require re-computation of the out-of-plane maneuver planning and requires careful evaluation depending on the computational constraints.

6. Conclusion

This paper has developed and validated an optimal multi-impulse control scheme for satellite formation flying using Relative Orbital Elements (ROE), with a particular focus on accounting for both secular J_2 perturbations and the effects of an eccentric chief orbit. The ROE framework has been demonstrated to be effective for formulating control strategies that are fuel-efficient and computationally viable, making it well-suited for onboard implementation in future space missions.

This work addresses a significant gap in the literature by tackling the combined challenges of J_2 perturbations and orbit eccentricity, which, although, the previous research has included both effects in the computation of the pseudostate, it has nevertheless treated them independently in the impulsive maneuver planning stage. Numerical simulations and comparative analysis demonstrate that the proposed control schemes significantly improve the accuracy of formation reconfigurations compared to previously established methods [4]. Furthermore, this study evaluates the cross-coupling effects between in-plane and out-of-plane elements arising from the use of the J_2-perturbed STM and the control input matrix for eccentric orbits. The findings indicate that the dominant source of cross-coupling is the control input matrix, and its impact can be mitigated by sequentially performing out-of-plane maneuver planning followed by in-plane maneuver planning.

Future research could explore the integration of additional perturbative forces, such as atmospheric drag and solar radiation pressure, with an emphasis on incorporating higher-fidelity STMs into control schemes for eccentric orbits asides from simply considering them in the pseudostate computation. Aside from simply considering them in the pseudo-state computation. Furthermore, ensuring safe formation configurations during reconfigurations and assessing the computational efficiency of these algorithms are essential areas for further study. Refining their implementation for real-time onboard applications will also be a critical step forward.

In conclusion, this paper presents a novel, robust, and efficient solution to the challenges of formation flying, paving the way for more

autonomous and longer-duration satellite missions with reduced reliance on ground intervention.

CRediT authorship contribution statement

Wei-Ting Chien: Writing – review & editing, Writing – original draft, Visualization, Validation, Software, Methodology, Investigation, Formal analysis, Conceptualization. **Afonso Botelho:** Writing – review & editing, Supervision, Resources, Methodology, Investigation, Conceptualization. **Bruno Ribeiro:** Writing – review & editing, Supervision, Methodology, Conceptualization. **Kieran Hayward:** Project administration. **Leonard Felicetti:** Writing – review & editing, Supervision.

Declaration of competing interest

The authors declare that they have no known competing financial interests or personal relationships that could have appeared to influence the work reported in this paper.

Acknowledgements

The authors gratefully acknowledge the support of Cranfield University and Deimos Space for the development of this research.

Data availability

No data was used for the research described in the article.

References

[1] S. D'Amico, Autonomous formation flying in low Earth orbit. PhD thesis, Technical University of Munich, 2010.
[2] G. Gaias, S. D'Amico, Impulsive maneuvers for formation reconfiguration using relative orbital elements, J. Guid. Control Dyn. 38 (6) (2015) 1036–1049, https://doi.org/10.2514/1.G000189.
[3] L. Riggi, S. D'Amico, Optimal impulsive control for spacecraft relative motion using non- linear models, in: Proceedings of the American Control Conference (ACC), 2015 url, https://slab.sites.stanford.edu/sites/g/files/sbiybj25201/files/media/file/space2016_chernickdamico.pdf. Accessed: Mar. 7, 2026.
[4] M. Chernick, S. D'Amico, New closed-form solutions for optimal impulsive control of spacecraft relative motion, in: AIAA Space and Astronautics Forum and Exposition (SPACE 2016), 2016 url: https://slab.sites.stanford.edu/sites/g/files/sbiybj25201/files/media/file/space2016_chernickdamico.pdf. Accessed: Mar. 7, 2026.
[5] D.A. Vallado, Fundamentals of Astrodynamics and Applications, 4th., Microcosm Press, 2013, p. 636. Chap. General Perturbation Techniques.
[6] A. Koenig, M. Guffanti, S. D'Amico, New State transition matrices for spacecraft relative motion in perturbed orbits, J. Guid. Control Dyn. 40 (8) (2017) 1989–2001, https://doi.org/10.2514/1.G002298.
[7] D. Chernick, S. D'Amico, Design and analysis of a novel relative sensor system for autonomous rendezvous and docking, in: AAS/AIAA Space Flight Mechanics Meeting, American As- tronautical Society (AAS), American Institute of Aeronautics, and Astronautics (AIAA), Kauai, Hawaii, Feb. 2018.
[8] N. Delurgio, S. D'Amico, Closed-form modeling and control of spacecraft swarms in eccentric orbits, in: 2024 IEEE Aerospace Conference, IEEE, March 2, 2024, pp. 1–20, https://doi.org/10.1109/AERO58975.2024.10521046.
[9] T. Sasaki, Linear time/parameter-varying models with relative orbit elements considering continuous controllability, J. Guid. Control Dyn. 48 (1) (2025) 177–191, https://doi.org/10.2514/1.G008297.
[10] T.V. Peters, Guidance for Rendezvous and Formation Flying in Elliptical Orbits, Delft University of Technology, 2024, https://doi.org/10.4233/uuid:76aad116-9a1b-4f8a-a289-4727ea10e709. PhD.
[11] M. Hunter, S. D'Amico, Robust closed-form framework for drag-propulsive control of formation flight, in: 2024 IEEE Aerospace Conference, IEEE, 2024, https://doi.org/10.1109/AERO58975.2024.10521029.
[12] M. Willis, S. D'Amico, Analytical description of relative position and velocity on J_2-perturbed eccentric orbits, in: AAS/AIAA Space Flight Mechanics Meeting, 2021 url: https://slab.sites.stanford.edu/sites/g/files/sbiybj25201/files/media/file/aas_2021_relative_motion_on_j2_perturbed_eccentric_orbits_final_.pdf. Accessed: Mar. 7, 2026.
[13] B. Kuiack, S. Ulrich, Nonlinear analytical equations of relative motion on J_2-perturbed eccentric orbits, J. Guid. Control Dyn. 41 (12) (2018) 2664–2675, https://doi.org/10.2514/1.G003723.
[14] L. Cao, X. Chen, Minimum sliding mode error feedback control for inner-formation satellite system with J_2 and small eccentricity, Sci. China Inf. Sci. 59 (2016) 072203, https://doi.org/10.1007/s11432-016-5573-1.
[15] M. Sabatini, D. Izzo, G. Palmerini, Minimum control for spacecraft formations in a J_2-perturbed environment, Celest. Mech. Dyn. Astron. (2009), https://doi.org/10.1007/s10569-009-9214-5.
[16] P. Sengupta, S.R. Vadali, K.T. Alfriend, Averaged relative motion and applications to formation flight near perturbed orbits, J. Guid. Control Dyn. (2008), https://doi.org/10.2514/1.30620.



https://dspace.org/

Semi-analytical formation-flying control in J2-perturbed eccentric orbits

Chien, Wei-Ting; Botelho, Afonso; Ribeiro, Bruno; Hayward, Kieran; Felicetti, Leonard

2026-10
Elsevier
https://doi.org/10.1016/j.ast.2026.112247
Chien W-T, Botelho A, Ribeiro B, et al., (2026) Semi-analytical formation-flying control in J2-perturbed eccentric orbits. Aerospace Science and Technology, Volume 177, Part A, October 2026, Article number 112247

Downloaded from a DSpace repository. https://dspace.org/